Geophysical Research Letters

RESEARCH LETTER
10.1029/2022GL101392

Quantifying Flow Velocities in River Deltas via Remotely Sensed Suspended Sediment Concentration

Carmine Donatelli[1,2], Paola Passalacqua[1], Kyle Wright[1], Gerard Salter[3], Michael P. Lamb[3], Daniel Jensen[4], and Sergio Fagherazzi[2]

[1]Department of Civil, Architectural and Environmental Engineering, University of Texas at Austin, Austin, TX, USA, [2]Department of Earth and Environment, Boston University, Boston, MA, USA, [3]Division of Geological and Planetary Sciences, California Institute of Technology, Pasadena, CA, USA, [4]Jet Propulsion Laboratory, California Institute of Technology, Pasadena, CA, USA

Key Points:

- We propose a novel methodology to compute water fluxes and flow velocities in deltas from maps of suspended sediment concentration
- Our method quantifies flow velocities based on the distance between streaklines, under the assumption that streaklines act as streamlines
- Flow velocities obtained via our methodology match well with those derived from a numerical model in a sub-region of the Wax Lake Delta

Supporting Information:

Supporting Information may be found in the online version of this article.

Correspondence to:

C. Donatelli,
dcarmine@bu.edu

Citation:

Donatelli, C., Passalacqua, P., Wright, K., Salter, G., Lamb, M. P., Jensen, D., & Fagherazzi, S. (2023). Quantifying flow velocities in river deltas via remotely sensed suspended sediment concentration. *Geophysical Research Letters*, *50*, e2022GL101392. https://doi.org/10.1029/2022GL101392

Received 23 SEP 2022
Accepted 4 FEB 2023

Abstract Deltas are fragile ecosystems threatened by sea-level rise, sediment starvation, and subsidence. Erosional/depositional processes in these systems mainly depend on the sediment supply and the spatial divergence in bed shear stress induced by hydrodynamic forces. Thus, quantifying the spatiotemporal variability of the flow velocity field is essential for forecasting their fate. To calibrate/validate models, field measurements alone are not sufficient because such data only characterize the hydrodynamic conditions in localized areas. Remote sensing has potential to fill this data gap. We developed a methodology to estimate flow velocities from a map of suspended sediment concentration (SSC) measured by the NASA airborne spectrometer AVIRIS-NG within the Wax Lake Delta, Louisiana. We extracted streaklines from remotely sensed SSC estimates, and quantified water fluxes and velocities based on the distance between them. Our study demonstrates that the velocity field in deltas can be estimated by leveraging the synoptic information offered by remote sensing.

Plain Language Summary River deltas are coastal environments particularly susceptible to sea-level rise. Sediment deposition can counteract land loss from sea-level rise, but we have a poor understanding of where and when land is built through sediment accretion. Improving the accuracy of hydrodynamic models is pivotal to predicting the fate of sediment that rebuilds sinking land, but we lack methods to test these models against observations over large areas. Here, we introduce a new method to measure water discharge, flow direction and speed from remotely sensed data. The method takes advantage of water flow patterns revealed in data collected from a NASA instrument flown on an airplane. Our study shows the utility of remotely sensed data to improve the performance and reliability of models that are needed to predict the fate of river deltas.

1. Introduction

River deltas are dynamic coastal environments characterized by distributary channels and deltaic islands. The channel network in these systems is composed by primary and secondary channels, with both playing a fundamental role in carrying water, sediments, and nutrients to deltaic islands (e.g., Edmonds & Slingerland, 2007; Edmonds et al., 2011; Syvitski, 2006; Salter & Lamb, 2022). The importance of water connectivity, defined by Freeman et al. (2007) as the water-mediated transport of matter, energy and organisms across different elements of a landscape, has been emphasized in several studies (e.g., Bracken et al., 2013; Tetzlaff et al., 2007; Wohl et al., 2018). For instance, Hiatt and Passalacqua (2015) explored the connectivity through the delta network of channels and islands in the Wax Lake Delta (WLD) in coastal Louisiana, by measuring the hydrological exchange between these two morphological elements. Their field-based observations revealed that roughly 50% of the discharge is distributed from primary channels to islands via secondary channels and overbank flow. Subsequently, this finding was corroborated by other research (e.g., Liang et al., 2015, 2016). However, assessing how water fluxes vary spatially at larger scales is more difficult to achieve due to lack of synoptic hydrodynamic data. In fact, pursuing field measurements in vast areas of a river delta is time-consuming and costly (e.g., Dong et al., 2020).

Remote sensing can be used to fill this gap (e.g., Alsdorf et al., 2007; Altenau et al., 2017; Dogliotti et al., 2015; Paris et al., 2016), and it could offer a systemwide view of how a certain hydrodynamic quantity changes across the entire landscape. For instance, flow velocities in riverine environments have been estimated from remotely

sensed data using Particle Image Velocimetry (Muste et al., 2008). The purpose of this study is to evaluate spatial changes in flow velocities within deltas via remote sensing imagery. Specifically, we aim to employ remotely sensed images of suspended sediment concentration (SSC) to quantify water fluxes and flow acceleration/deceleration within the transition area between laterally confined flow and unchannelized delta front. This transition is particularly important for depositional/erosional patterns that ultimately control the long-term channel extension and delta progradation (e.g., Hiatt & Passalacqua, 2017; Shaw et al., 2018).

Previous studies employed remotely sensed SSC data to study depositional/erosional processes in river deltas (e.g., Jensen et al., 2019). For instance, Salter et al. (2022) linked changes in SSC along streaklines, that is, curves defined by the paths of all fluid particles that have passed through a specific spatial location over time (Kundu et al., 2011), to patterns of sediment deposition and erosion. Specifically, they used SSC data from remote sensing to locate streaklines, which were combined with flow velocities derived from a numerical model to evaluate SSC variations along these curves. However, a reliable methodology which enables the computation of the velocity field from the same SSC map is still missing. Such information would allow us to quantify instantaneous sediment fluxes in river deltas using a single remotely sensed image (i.e., without employing numerical models to derive the hydrodynamic field). In addition, this methodology has the potential to provide high-spatial resolution data over the entire river delta, which are needed to calibrate hydrodynamic models and obtain reliable predictions of the impact of sea level rise and engineering projects on these valuable coastal systems.

To the best of our knowledge, few attempts are present in the literature to derive flow velocities from optical remote sensing products (e.g., Bowen et al., 2002; Chen et al., 2008; Muste et al., 2008; Yang et al., 2015). Ayoub et al. (2018) conducted an airborne L-band synthetic aperture radar acquisition campaign to quantify current velocities within the WLD. However, flow speeds were only estimated over the shallow vegetated deltaic islands. In this paper, we want to fill this gap by providing a methodology that can help compute the flow field for the remainder of the river delta. In particular, we propose a new approach to calculate flow partitioning among different parts of the delta, and related velocities, from maps of remotely sensed SSC derived from images obtained by an airborne hyperspectral instrument.

Our method takes advantage of curvilinear patterns of high and low sediment concentrations, known as streaklines, derived from an AVIRIS-NG image (Salter et al., 2022). We use the WLD, a river delta with a bifurcating distributary channel network, as a test case. We assume that the flow traced by the streaklines is steady, that is, its pattern does not change over time (Cathcart et al., 2020; Shaw et al., 2016). This condition implies that streaklines correspond with streamlines (i.e., curves tangential to the local fluid velocity), and water fluxes and flow velocities can be quantified based on the distance between these curves. To test the reliability of the proposed methodology, the flow velocities computed from remote sensing data are compared with high-resolution numerical modeling results obtained by means of the ANUGA numerical framework (Roberts et al., 2015) and calibrated for the WLD (Wright et al., 2022). This study shows a generalized approach which utilizes streaklines to compute the velocity field in river deltas. The proposed methodology offers the possibility to evaluate the spatial variability of hydrodynamic conditions within river deltas by leveraging the spatial information available in remotely sensed data.

2. Methods

We use streaklines to compute water discharges and flow velocities within a sub-region of the WLD. First, we extract streaklines from a map of remotely sensed SSC (Figure 1a, see Section 2.1). Then, to compute water fluxes and related flow velocities from these curves, we assume that streaklines are steady in time (hereinafter called steady streaklines or streamlines) and representative of the depth-averaged flow conditions (see subsection 2.2). These assumptions are discussed in Shaw et al. (2016) and Cathcart et al. (2020), who demonstrate that three-dimensional flow patterns (e.g., due to winds) and unsteady variations (e.g., due to tides) can be neglected under certain conditions in the WLD (e.g., when the water discharge is greater than 2,400 m^3/s with stable or falling tides). In general, we can assume steady conditions if the hydrodynamic conditions change slowly in time. Assuming that multiple images of SSC are available within a tidal cycle, the validity of this assumption can be assessed by extracting streaklines from each image and checking whether their locations vary over time. If such temporal changes are negligible over one or 2 hr, then steady conditions can be assumed over that time period. Finally, we compare the flow velocities obtained via remote sensing with numerical modeling results along a streamtube, that is, a tubular region of fluid surrounded by two streamlines (e.g., Durst, 2022).

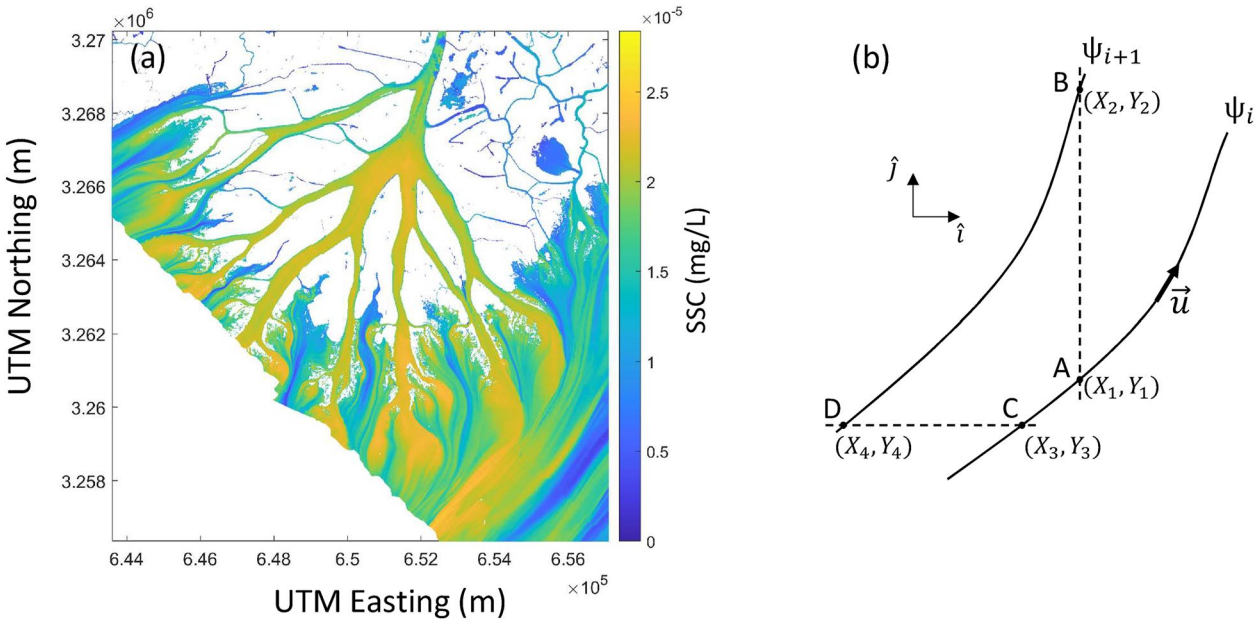

Figure 1. (a) Map of remotely sensed suspended sediment concentration over Wax Lake Delta, Louisiana. Data from Jensen et al. (2019, 2021), based on AVIRIS-NG flyover from 18 October 2016 between 15:25 and 15:41 GMT. (b) Schematic representation of two closely-spaced steady streaklines.

2.1. Streaklines Extraction

In this subsection, we describe how to extract streaklines via the semi-automated method proposed by Salter et al. (2022). Curvilinear patterns in AVIRIS-NG (i.e., streaklines) arise from the contrast between waters characterized by low SSC coming from deltaic islands, and waters characterized by high SSC coming from channels (Salter et al., 2022). These curves may differ from the streaklines detected via radar and employed in previous studies to estimate flow directions in the WLD (Cathcart et al., 2020; Shaw et al., 2016). In fact, curvilinear features in radar imagery are related to the presence of biofilms on the water surface. Specifically, such biofilms alter both the emissivity and roughness of the water surface, making them easily detectable via remote sensing.

We use a map of remotely sensed SSC (Jensen et al., 2021) developed by Jensen et al. (2019) from the 18 October 2016 AVIRIS-NG (Airborne Visible/Infrared Imaging Spectrometer-Next Generation) flyover of WLD, Louisiana, that occurred between 15:25 and 15:41 GMT (Figure 1a). This map is based on a collection of paired SSC and remote sensing reflectance values (Rrs) measured at the water surface with a field spectrometer. The first derivatives of the in situ Rrs values, convolved to AVIRIS-NG's spectral resolution, were used to generate a Partial Least Squares Regression model for SSC. A refined selection of the derivative bands formed the final model inputs based on variable importance scores. The model attained an R^2 of 0.83, with a mean relative error of 14.87% and a mean absolute error of 6.34 mg/L, calculated from the 2016 AVIRIS-NG SSC products, with additional independent validation sites showing low-error SSC retrievals (Jensen et al., 2019).

First, a Perona-Malik filter is applied to the original data to remove noise (i.e., irregularities at scales smaller than the one of interest) and preserve the original image's sharp-gradient features (Perona & Malik, 2010). This smoothing is also critical to make the calculations (e.g., derivatives) mathematically well posed (Passalacqua et al., 2010). Next, we compute the geometric curvature (i.e., divergence of the normalized gradient) of SSC, which is interpreted as the curvature of the SSC contour lines (i.e., lines connecting points of equal SSC). More specifically, the geometric curvature (κ) of a generic function ϕ: $\mathbb{R}^2 \rightarrow \mathbb{R}$ can be expressed as follows (Minar et al., 2020):

$$\kappa = \nabla \cdot \frac{\nabla \phi}{|\nabla \phi|} = \frac{\phi_{xx}\phi_y^2 - 2\phi_x\phi_y\phi_{xy} + \phi_{yy}\phi_x^2}{\left(\phi_x^2 + \phi_y^2\right)^{3/2}} \quad (1)$$

We then define a cost function (η), which represents the cost of traveling between the streaklines' start and end points in terms of SSC and geometric curvature. In particular, this cost function is defined as in Salter et al. (2022):

$$\eta = \begin{cases} 1 - e^{-k_1 \kappa} + e^{-k_2 c}, & \text{for high concentration streaks.} \\ 1 - e^{k_1 \kappa} + e^{k_2 (c - \max(c))}, & \text{for low concentration streaks.} \end{cases} \quad (2)$$

where c is the SSC, while k_1 and k_2 are parameters controlling how well the curves of minimum cost follow the curvature and the concentration fields (these parameters are obtained by trial-and-error). These parameters can be selected at the beginning of the analysis using a few test streaklines; a poor choice of k_1 and k_2 is visually obvious as an extracted streakline that deviates from the real one (Salter et al., 2022). Once these two parameters have been set, all streaklines are extracted using the same values of k_1 and k_2. Note that we used a map of SSC in this study, but one could also employ a simple image-derived quantity that highlights spatial differences in water color and could thus serve as a proxy for SSC. However, extracting such a signal from these images would not be trivial and by using SSC we were able to build upon previous work that has already validated the approach.

Finally, we identify the streaklines as geodesic curves (i.e., curves of minimum cost), by computing the geodesic distance of each pixel from the start point and detecting the geodesic curve by following the steepest descendant path from the end point to the start point. The methodology is semi-automated since the start and end points here are defined manually from an image of curvature. More specifically, streaklines are identified visually from the map of geometric curvature, and endpoints are selected as the points where curvilinear features either terminate or become ambiguous. Further details of the method can be found in Salter et al. (2022).

2.2. Water Discharges and Flow Velocities

Once the streaklines are extracted, we compute flow velocities under steady-state conditions. This assumption implies that streaklines, streamlines and pathlines (i.e., trajectories that individual water parcels follow) coincide with each other. In particular, we quantify flow velocities (and related water discharges) using three fundamental proprieties (for example, Durst, 2022): (a) the difference between the values of a stream function (i.e., a scalar function whose derivative with respect to any direction gives the velocity component at right angles to that direction) over two streamlines is proportional to the water flow rate across any section crossing the two curves (e.g., section AB or CD in Figure 1b), (b) closely-spaced streamlines create impermeable tubes (i.e., the discharge does not change along their length), and (c) water fluxes are proportional to the distance between streamlines under the assumption of uniform flow.

Under steady state conditions, the continuity equation in shallow waters reads:

$$\frac{\partial(\mathrm{hu})}{\partial x} + \frac{\partial(\mathrm{hv})}{\partial y} = 0 \quad (3)$$

where h is the water depth, and the 2D vector (u,v) is the fluid's horizontal flow velocity. This equation can be re-written as follows:

$$\frac{\partial(q_x)}{\partial x} + \frac{\partial(q_y)}{\partial y} = 0 \quad (4)$$

where q_x and q_y represent the discharge per unit width in the x- and y-direction. A scalar function (ψ), called stream function, can be defined over the steady streaklines. In particular, the discharge per unit width (q) in the x- and y-direction can be expressed in terms of the stream function (e.g., Fagherazzi, 2002):

$$q_x = hu = \frac{\partial \psi}{\partial y}, q_y = hv = -\frac{\partial \psi}{\partial x} \quad (5)$$

Next, we consider two closely-spaced streamlines and we quantify the water flux (Q) through section AB (Figure 1b):

$$Q_{\mathrm{AB}} = \int_{y1}^{y2} q_x \, dy = \int_{y1}^{y2} \frac{\partial \psi}{\partial y} dy \quad (6)$$

Since the total derivative of ψ along AB (dx = 0) is equal to:

$$\mathrm{d}\psi = \frac{\partial \psi}{\partial y}\, dy \tag{7}$$

expression Equation 6 reads:

$$Q_{AB} = \int_{y1}^{y2} \mathrm{d}\psi = \psi_{i+1} - \psi_i \tag{8}$$

This means that the difference in the stream function values between two curves gives the water volume flow rate. The same result can be obtained for any other section (e.g., CD in Figure 1b). Since we are interested in knowing how the stream function varies among these curves to obtain water discharges (i.e., $\psi_{i+1} - \psi_i$), we can assume a null value or an arbitrary constant over a specific curve. After assigning the values of the stream function along the steady streaklines (assuming the existence of a uniform flow downstream of the delta), the discharge Q_i (i.e., $\psi_{i+1} - \psi_i$) can be computed and divided by the streamtube's cross-sectional area to obtain along-streamtube velocities (i.e., average velocities in each cross-section). This derivation is equivalent to writing the conservation of mass along a streamtube, and then computing the velocity magnitude knowing the streamtube's geometry and the velocity across a generic section. Note that prior knowledge of the bathymetry is required to compute flow velocities (bathymetric data for the WLD come from Denbina et al. (2020)). In the absence of bathymetric information, this method can still be applied to characterize the spatial distribution of discharge in the delta (note that discharges have absolute units even if bathymetry is not available).

3. Results and Discussion

3.1. Computation of Flow Velocities via Remote Sensing

The geometric curvature (κ) is computed within a sub-region of the WLD (Figure 2a) and it exhibits positive and negative values. In particular, low concentration curves (troughs) have a positive κ, whereas high concentration curves (peaks) show a negative geometric curvature. Start and end points are manually selected from this, and connected by geodesics (curves of minimum cost). The streaklines overlaying the map of remotely sensed SSC are depicted in Figure 2b. In general, the streamtubes' width can vary due to variations in the velocity magnitude or water depth or both. We follow three steps for quantifying the flow velocity magnitude from the steady streaklines: (a) assign a value of the stream function along each streakline, (b) compute the water flux (Q) for each streamtube based on the stream function values, and (c) divide Q by the streamtube's cross-sectional area (assuming a known bathymetry and water surface elevation).

We assume the existence of a uniform flow field downstream of the delta, and we assign a null value of the stream function along the westernmost streakline (Figure 2b). This choice does not impact the results since Q is proportional to changes in stream function's values. Once the stream function is assigned along each steady streakline, a quantity proportional to the water flux is obtained from the difference in the stream function values between these curves. We note that, in general, we cannot compute the exact stream function, but a function which scales with the real one (unless the velocity is known in a certain section). Here, to obtain the exact stream function, we assigned the velocity resulted from the numerical model downstream of the delta. This type of information is not essential, however, because one can derive a velocity field which is proportional to the real one even if such data are not available. The values assumed by the stream function along four arbitrary curves (dashed curves in Figures 2b and 2c) are depicted in Figure 2c, while the water flow rate for each streamtube is shown in Figure 2d.

At this point, we compute the flow velocities in three different sections along streamtube 5 (i.e., white dashed lines in Figure 2b). The flow velocity magnitude in section a-a is 0.35 m/s, then it decreases to 0.24 m/s in section b-b and finally reaches 0.2 m/s in section c-c. This means that the flow speed within the primary channel decreases as soon as it enters the shallow transition zone between confined and unconfined flow (consequently the streamtube's width increases). When water depths start to increase again (for bathymetric information see Figure 3b), the flow velocity slightly decreases (the streamtube's width decreases within this region since water depths become greater, whereas the flow velocity magnitude remains fairly constant with respect to section b-b). This finding is broadly consistent with Shaw et al. (2016) who found that adverse bed slopes are associated with flow direction divergences, while the flow converges where water depths increase.

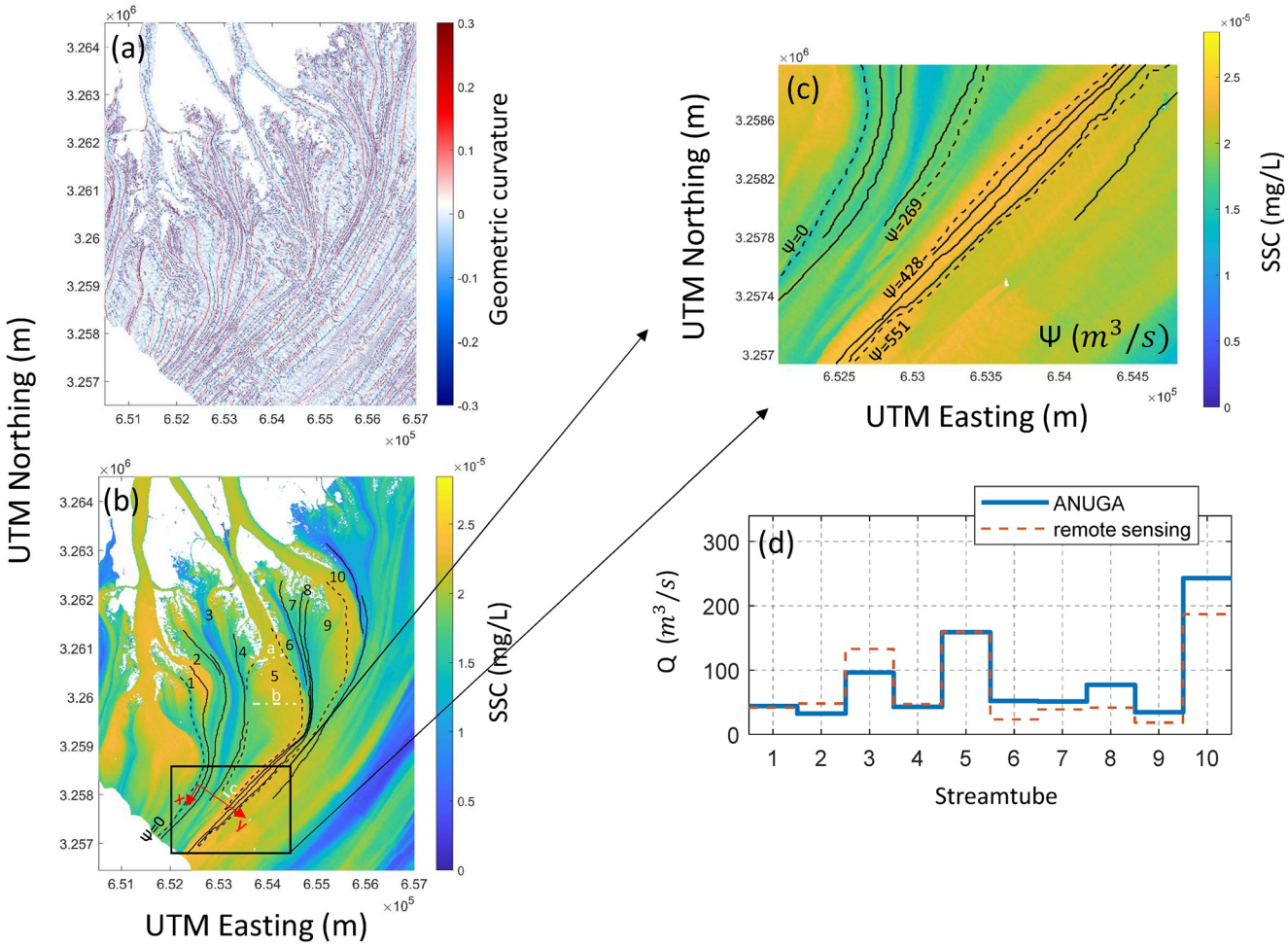

Figure 2. (a) Geometric curvature (κ) of remotely sensed suspended sediment concentration (SSC). (b) Extracted streaklines overlaying the map of SSC. (c) Stream function values along four steady streaklines (dashed curves). (d) Discharge correspondences between the model and the estimates for each streamtube.

3.2. Validation of the Methodology

We simulate the hydrodynamics in the WLD by employing the ANUGA numerical model (Roberts et al., 2015), which uses the finite volume method to solve the 2D depth-averaged shallow water equations. The model was calibrated for the WLD in Wright et al. (2022) and it was shown to match observations well. The numerical domain is partitioned by an unstructured mesh of triangular grid cells. Details on the forcing conditions, set up and model validation can be found in Wright et al. (2022).

To validate our approach, we compare the instantaneous discharges and flow velocities computed from the map of SSC with those obtained from the numerical model ANUGA (Wright et al., 2022). Discharge correspondences between the model and the estimates are depicted in Figure 2d. The velocity magnitude at the time of the AVIRIS-NG flight is shown in Figure 3a. We also reported the two steady streaklines delimiting streamtube 5 (Figure 3a) and the bathymetry of the selected streamtube (Figure 3b) in Figure 3. Along-streamtube velocities (i.e., average velocities in each cross-section) are computed from the numerical model results (Figure 3a). These velocities match well those derived with our streamtube method (root-mean-square error, $\epsilon_{\mathrm{rms}} = 0.06$ m/s), although the velocity profiles do not overlap exactly (Figure 3c, see also Figure S1). We explain this discrepancy and the limitations of our approach in the next subsection.

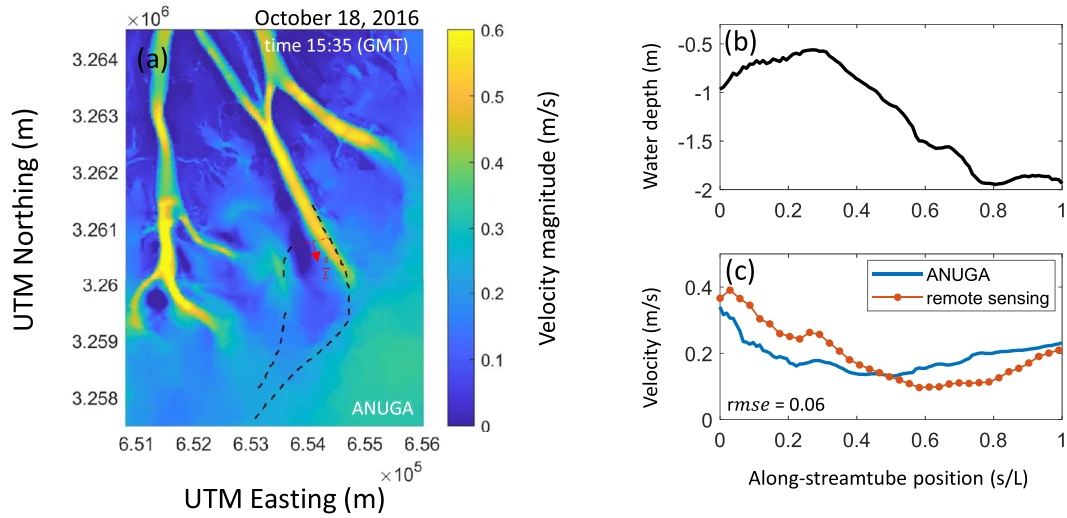

Figure 3. (a) Instantaneous velocity magnitude at the time of the AVIRIS-NG flight computed with the numerical model ANUGA. The streamtube 5 is reported in the same figure. (b) Bathymetry of streamtube 5. (c) Remote sensed and simulated velocities along streamtube 5. For this plot the root-mean-square error (rmse) is indicated.

3.3. Strengths and Limitations of the Proposed Methodology

This study presents a novel methodology to measure water discharge, flow direction and speed from remotely sensed data. The described approach can provide high-spatial resolution hydrodynamic data, which would allow us to test numerical models against observations over large areas of river deltas. More specifically, the velocity field obtained from remotely sensed data can be utilized to constrain crucial model parameters, and improve the accuracy and performance of numerical simulations. This is needed to achieve reliable estimations of fluxes of water (and its constituents), and predict the fate of sediment that rebuilds sinking land. Furthermore, our methodological framework can be applied to other systems worldwide where maps of SSC and bathymetric information are available, although bathymetric data are only needed to compute flow velocities.

We assumed steady-state conditions to apply the streamlines' theory. This assumption was tested and discussed in Cathcart et al. (2020), where in-situ flow direction measurements were compared with remotely sensed flow directions estimated though the use of steady streaklines. Ayoub et al. (2018) and Cathcart et al. (2020) showed that this assumption holds in the WLD, although differences between measurements and remotely sensed values vary as a function of the forcing conditions. Specifically, the best match between steady streaklines and in-situ measurements was obtained during large discharges with stable or falling tides, whereas the largest mismatch took place during rising tides at a rate greater than 0.07 m/hr (Cathcart et al., 2020). In fact, Cathcart et al. (2020) argue that when the rate of tidal change becomes large, the assumption of steady state conditions does not hold and differences between streaklines and flow velocity patterns increase.

During the 18 October 2016 AVIRIS-NG flight tides were falling and water discharge was 1,900 m^3/s. Such hydraulic conditions are not optimal to assume a steady flow, however results may be still acceptable (the agreement between streakline-derived flow and measurements ranges between fair to optimal for water discharges at Calumet between 1,000 and 7,000 m^3/s, and a rate of tidal change between −0.075 and 0.03 m/hr) (Cathcart et al., 2020). This implies that the streaklines might not be perfectly tangential to the flow direction (i.e., the tubes detected by these curves are not perfectly impermeable) during the studied period, which in turn could affect the velocity magnitude computed via our method (Figure 3c). In fact, the SSC becomes more uniform downstream of the delta suggesting that water masses are exchanged among streamtubes within this part of the domain (Figure 2c). In addition, our approach does not consider secondary currents due to baroclinic effects and/or winds which may alter the velocity profile along the vertical direction (e.g., Gerkema, 2019; Valle-Levinson, 2010). This point was extensively discussed in Shaw et al. (2016), who found that the flow direction at the top layer of the water column and the depth-averaged flow direction measured by acoustic Doppler current profiler were aligned in the WLD during the period of observation characterized by high discharge conditions. Furthermore,

Cathcart et al. (2020) found no clear relationship between wind direction and streakline direction which suggests that the streakline-derived flow is representative of the depth-averaged flow conditions also during wind events.

Finally, it is worth highlighting that our results represent a snapshot of the flow characteristics in the selected streamtube. A sequence of streaklines obtained with several images of SSC at different instants could provide information on the temporal variability of the flow, if the SSC images have a sufficient resolution to capture the streaklines. The presence of streaklines also depends on hydrodynamic conditions (e.g., waves, tides) and gradients in sediment concentration. Short-term events (e.g., storms) can dramatically alter water movements and the amount of sediment in suspension in the system (e.g., Donatelli et al., 2022a, 2022b; Duran-Matute et al., 2016) which can inhibit the presence of streaklines (Salter et al., 2022).

4. Conclusions

In this study, we provide a general framework to compute discharge and flow velocities via remote sensing imagery in river deltas. The main conclusions of this paper are.

1. The spatial distribution of discharge can be computed from a map of remotely sensed sediment concentration. We extracted the steady streaklines via a semi-automated method, and we estimated water fluxes based on the distance between these curves under the assumption of uniform flow. The described methodology can be applied to other river deltas worldwide if the sediment maps are available. Note that for computing the discharge, bathymetric data are not necessary.
2. If bathymetric data are available, flow velocities can be derived as the ratio between discharge per unit length and water depth.
3. The proposed approach was tested with high-resolution numerical modeling results carried out by means of the numerical model ANUGA. We found that the results computed via remote sensing match well with those obtained through the numerical model along a streamtube.
4. The present study highlights the importance of remote sensing to understand river deltas' dynamics at large scales, since this methodology has the potential to offer high-resolution hydrodynamic data over vast regions. These data are important to comprehend water movements in these systems.
5. The velocity field obtained from a map of remotely sensed SSC can be used to improve the accuracy of numerical models, and precisely quantify fluxes of water, sediments and nutrients that are essential to determining the resilience of river deltas to environmental change.

Data Availability Statement

Suspended sediment concentration data can be downloaded from the ORNL DAAC (https://doi.org/10.3334/ORNLDAAC/1822). Bathymetric data and flow velocities can be downloaded from https://doi.org/10.5281/zenodo.7504497.

Acknowledgments
We thank the Editor and the two anonymous Reviewers for their comments. This work within NASA Delta-X project, is funded by the Science Mission Directorate's Earth Science Division through the Earth Venture Suborbital-3 Program NNH17ZDA001N-EVS3. S.F. was also partly funded by the USA National Science Foundation awards 2224608 (PIE LTER), 1832221 (VCR LTER).

References

Alsdorf, D., Bates, P., Melack, J., Wilson, M., & Dunne, T. (2007). Spatial and temporal complexity of the Amazonflood measured from space. *Geophysical Research Letters*, *34*(8), L08402. https://doi.org/10.1029/2007GL029447

Altenau, E. H., Pavelsky, T. M., Moller, D., Lion, C., Pitcher, L. H., Allen, G. H., et al. (2017). Airswot measurements of river water surface elevation and slope: Tanana River, AK. *Geophysical Research Letters*, *44*(1), 181–189. https://doi.org/10.1002/2016GL071577

Ayoub, F., Jones, C. E., Lamb, M. P., Holt, B., Shaw, J. B., Mohrig, D., & Wagner, W. (2018). Inferring surface currents within submerged, vegetated deltaic islands and wetlands from multi-pass airborne SAR. *Remote Sensing of Environment*, *212*, 148–160. https://doi.org/10.1016/j.rse.2018.04.035

Bowen, M. M., Emery, W. J., Wilkin, J. L., Tildesley, P. C., Barton, I. J., & Knewtson, R. (2002). Extracting multiyear surface currents from sequential thermal imagery using the maximum cross-correlation technique. *Journal of Atmospheric and Oceanic Technology*, *19*, 10–1676. https://doi.org/10.1175/1520-0426(2002)019<1665:emscfs>2.0.co;2

Bracken, L., Wainwright, J., Ali, G., Tetzlaff, D., Smith, M., Reaney, S., & Roy, A. (2013). Concepts of hydrological connectivity: Research approaches, pathways and future agendas. *Earth-Science Reviews*, *119*, 17–34. https://doi.org/10.1016/j.earscirev.2013.02.001

Cathcart, C., Shaw, J., & Amos, M. (2020). Validation of streaklines as recorders of synoptic flow direction in a deltaic setting. *Remote Sensing*, *12*(1), 148. https://doi.org/10.3390/rs12010148

Chen, W., Mied, R. P., & Shen, C. Y. (2008). Near-surface ocean velocity from infrared images: Global optimal solution to an inverse model. *Journal of Geophysical Research*, *113*(C10), C004747. https://doi.org/10.1029/2008JC004747

Denbina, M., Simard, M., Pavelsky, T., Christensen, A., Liu, K., & Lyon, C. (2020). *Pre-Delta-X: Channel Bathymetry of the Atchafalaya Basin, LA, USA, 2016*. ORNL DAAC.

Dogliotti, A. I., Ruddick, K. G., Nechad, B., Doxaran, D., & Knaeps, E. (2015). A single algorithm to retrieve turbidity from remotely-sensed data in all coastal and estuarine waters. *Remote Sensing of Environment*, *156*, 157–168. https://doi.org/10.1016/j.rse.2014.09.020

Donatelli, C., Duran-Matute, M., Gräwe, U., & Gerkema, T. (2022a). Residual circulation and freshwater retention within an event-driven system of intertidal basins. *Journal of Sea Research*, *186*, 102242. https://doi.org/10.1016/j.seares.2022.102242

Donatelli, C., Duran-Matute, M., Gräwe, U., & Gerkema, T. (2022b). Statistical detection of spatio-temporal patterns in the salinity field within an inter-tidal basin. *Estuaries and Coasts*, *45*(8), 2345–2361. https://doi.org/10.1007/s12237-022-01089-3

Dong, T. Y., McElroy, J. A. N. B., Il'icheva, E., Pavlov, M., Ma, H., Moodie, A. J., et al. (2020). Predicting water and sediment partitioning in a delta channel network under varying discharge conditions. *Water Resources Research*, *56*(11), e2020WR027199. https://doi.org/10.1029/2020WR027199

Duran-Matute, M., Gerkema, T., & Sassi, M. G. (2016). Quantifying the residual volume transport through a multiple-inlet system in response to wind forcing: The case of the Western Dutch Wadden Sea. *Journal of Geophysical Research: Oceans*, *121*(12), 8888–8903. https://doi.org/10.1002/2016JC011807

Durst, F. (2022). *Fluid mechanics: An introduction to the theory of fluid flow*s. Springer Berlin Heidelberg. https://doi.org/10.1007/978-3-662-63915-3

Edmonds, D. A., Paola, C., Hoyal, D. C. J. D., & Sheets, B. A. (2011). Quantitative metrics that describe river deltas and their channel networks. *Journal of Geophysical Research*, *116*(F4), F04022. https://doi.org/10.1029/2010JF001955

Edmonds, D. A., & Slingerland, R. L. (2007). Mechanics of river mouth bar formation: Implications for the morphodynamics of delta distributary networks. *Journal of Geophysical Research*, *112*(F2), F02034. https://doi.org/10.1029/2006JF000574

Fagherazzi, S. (2002). Basic flow field in a tidal basin. *Geophysical Research Letter*s, *29*(8), 62-1–62-3. https://doi.org/10.1029/2001GL013787

Freeman, M. C., Pringle, C. M., & Jackson, C. R. (2007). Hydrologic connectivity and the contribution of stream headwaters to ecological integrity at regional scales. *Journal of the American Water Resources Association*, *43*(1), 5–14. https://doi.org/10.1111/j.1752-1688.2007.00002.x

Gerkema, T. (2019). *An introduction to tides*. Cambridge University Press. https://doi.org/10.1017/9781316998793

Hiatt, M., & Passalacqua, P. (2015). Hydrological connectivity in river deltas: The first-order importance of channel-island exchange. *Water Resources Research*, *51*(4), 2264–2282. https://doi.org/10.1002/2014WR016149

Hiatt, M., & Passalacqua, P. (2017). What controls the transition from confined to unconfined flow? Analysis of hydraulics in a coastal river delta. *Journal of Hydraulic Engineering*, *143*(6), 03117003. https://doi.org/10.1061/(ASCE)HY.1943-7900.0001309

Jensen, D., Simard, M., Cavanaugh, K., Sheng, Y., Fichot, C. G., Pavelsky, T., & Twilley, R. (2019). Improving the transferability of suspended solid estimation in wetland and deltaic waters with an empirical hyperspectral approach. *Remote Sensing*, *385*(13), 11. https://doi.org/10.3390/RS11131629

Jensen, D. J., Simard, M., Fichot, C. G., & Pavelsky, T. M. (2021). *Pre-Delta-X: AVIRIS-derived Total Suspended Solids Maps for MRD, LA, USA, 2015-2016*. ORNL DAAC. https://doi.org/10.3334/ORNLDAAC/1822

Kundu, P. K., Cohen, I. M., & Dowling, D. (2011). *Fluid mechanics* (5th ed.). Elsevier Academic Press.

Liang, M., Geleynse, N., Edmonds, D. A., & Passalacqua, P. (2015). A reduced-complexity model for river delta formation—Part 2: Assessment of the flow routing scheme. *Earth Surface Dynamics*, *3*(1), 87–104. https://doi.org/10.5194/esurf-3-87-2015

Liang, M., Van Dyk, C., & Passalacqua, P. (2016). Quantifying the patterns and dynamics of river deltas under conditions of steady forcing and relative sea level rise. *Journal Geophysical Research: Earth Surface*, *121*(2), 465–496. https://doi.org/10.1002/2015jf003653

Minar, J., Evans, I. S., & Jenco, M. (2020). A comprehensive system of definitions of land surface (topographic) curvatures, with implications for their application in geoscience modelling and prediction. *Earth-Science Reviews*, *211*, 103414. https://doi.org/10.1016/j.earscirev.2020.103414

Muste, M., Fujita, I., & Hauet, A. (2008). Large-scale particle image velocimetry for measurements in riverine environments. *Water Resources Research*, *44*(4), W00D19. https://doi.org/10.1029/2008wr006950

Paris, A., Paiva, R. C., Silva, J. S., Moreira, D. M., Calmant, S., Garambois, P. A., et al. (2016). Stage-discharge rating curves based on satellite altimetry and modeled discharge in the Amazon basin. *Water Resources Research*, *25*(16), 3447–3459. https://doi.org/10.1002/2014WR015716

Passalacqua, P., Trung, T. D., Foufoula-Georgiou, E., Sapiro, G., & Dietrich, W. E. (2010). A geometric framework for channel network extraction from lidar: Nonlinear diffusion and geodesic paths. *Journal of Geophysical Research*, *115*(F1), F01002. https://doi.org/10.1029/2009jf001254

Perona, P., & Malik, J. (1990). Scale-space and edge detection using anisotropic diffusion. *IEEE Transactions on Pattern Analysis and Machine Intelligence*, *12*(7), 629–639. https://doi.org/10.1109/34.56205

Roberts, S., Nielsen, O., Gray, D., Sexton, J., & Davies, G. (2015). ANUGA user manual, 1176 geoscience Australia.

Salter, G., & Lamb, M. P. (2022). Autocyclic secondary channels stabilize deltaic islands undergoing relative sea level rise. *Geophysical Research Letters*, *49*(15), e2022GL098885. https://doi.org/10.1029/2022GL098885

Salter, G., Passalacqua, P., Wright, K., Feil, S., Jensen, D., Simard, M., & Lamb, M. P. (2022). Spatial patterns of deltaic deposition/erosion revealed by streaklines extracted from remotely-sensed suspended sediment concentration. *Geophysical Research Letters*, *49*(11), e2022GL098443. https://doi.org/10.1029/2022GL098443

Shaw, J. B., Ayoub, F., Jones, C. E., Lamb, M. P., Holt, B., Wagner, R. W., et al. (2016). Airborne radar imaging of subaqueous channel evolution in Wax Lake Delta, Louisiana, USA. *Geophysical Research Letters*, *43*(10), 5035–5042. https://doi.org/10.1002/2016GL068770

Shaw, J. B., Estep, J. D., Whaling, A. R., Sanks, K. M., & Edmonds, D. A. (2018). Measuring subaqueous progradation of the Wax Lake Delta with a model of flow direction divergence. *Earth Surface Dynamics*, *6*(4), 1155–1168. https://doi.org/10.5194/esurf-6-1155-2018

Syvitski, J. P. M. (2006). The morphodynamics of deltas and their distributary channels. In G. Parker & M. García (Eds.), *River, coastal and estuarine morphodynamics: RCEM 2005: London* (pp. 143–150). Taylor and Francis Group.

Tetzlaff, D., Soulsby, C., Bacon, P. J., Youngson, A. F., Gibbins, C., & Malcolm, I. A. (2007). Connectivity between landscapes and riverscapes—A unifying theme in integrating hydrology and ecology in catchment science? *Hydrological Processes*, *21*(10), 1385–1389. https://doi.org/10.1002/hyp.6701

Valle-Levison, A. (2010). *Contemporary issues in estuarine physics*. Cambridge University Press.

Wohl, E., Brierley, D., Cadol, T. J., Coulthard, T., Covino, K. A., Fryirs, G., et al. (2018). Connectivity as an emergent property of geomorphic systems Earth. *Earth Surface Processes and Landforms*, *44*(1), 4–26. https://doi.org/10.1002/esp.4434

Wright, K., Passalacqua, P., Simard, M., & Jones, C. E. (2022). Integrating connectivity into hydrodynamic models: An automated open-source method to refine an unstructured mesh using remote sensing. *Journal of Advances in Modeling Earth Systems*, *14*(8), e2022MS003025. https://doi.org/10.1029/2022MS003025

Yang, H., Arnone, R., & Jolliff, J. (2015). Estimating advective near-surface currents from ocean color satellite images. *Remote Sensing of Environment*, *158*, 1–14. https://doi.org/10.1016/j.rse.2014.11.010